Electric-field control of spin waves at room temperature in multiferroic $BiFeO_3$

P. Rovillain, M. Cazayous, Y. Gallais, A. Sacuto, M. A. Méasson
Laboratoire Matériaux et Phénomènes Quantiques (UMR 7162 CNRS), Université Paris Diderot-Paris 7, 75205 Paris cedex 13, France

R. de Sousa
Department of Physics and Astronomy, University of Victoria,Victoria, B.C., Canada, V8W 3P6

D. Colson, A. Forget
Service de Physique de l'Etat Condensé, DSM/DRECAM/SPEC, CEA Saclay, IRAMIS, SPEC (CNRS URA 2464), F-91191 Gif sur Yvette, France

M. Bibes & A. Barthélémy
Unité Mixte de Physique CNRS/Thales, 1 av. A. Fresnel, Campus de l'Ecole Polytechnique, F-91767 Palaiseau, France et Université Paris-Sud, 91405 Orsay, France.

(Dated: October 14, 2010)

To face the challenges lying beyond current CMOS-based technology, new paradigms for information processing are required. *Magnonics*[1] proposes to use spin waves to carry and process information, in analogy with photonics that relies on light waves, with several advantageous features such as potential operation in the THz range and excellent coupling to spintronics[2]. Several magnonic analog and digital logic devices[3] have been proposed, and some demonstrated[4]. Just as for spintronics, a key issue for magnonics is the large power required to control/write information (conventionally achieved through magnetic fields applied by strip lines, or by spin transfer from large spin-polarized currents). Here we show that in $BiFeO_3$, a room-temperature magnetoelectric material[5], the spin wave frequency (>600 GHz) can be tuned electrically by over 30%, in a non-volatile way and with virtually no power dissipation. Theoretical calculations indicate that this effect originates from a linear magnetoelectric effect related to spin-orbit coupling induced by the applied electric field. We argue that these properties make $BiFeO_3$ a promising medium for spin wave generation, conversion and control in future magnonics architectures.

Magnetoelectric multiferroics possess coexisting magnetic and ferroelectric phases, with cross-correlation effects between magnetic and electric degrees of freedom[6]. As such, they can potentially be used to control spin-based properties by electric fields[7], with very low associated power dissipation. This feature appears promising not only for spintronics, in which information is encoded by the spin-polarization of the electrical current[8], but also for magnonics that use magnetic excitations (spin waves) for information processing[1]. Indeed, just as coupling between magnetic and ferroelectric order parameters exists in multiferroics, coupled spin and lattice excitations termed electromagnons have also been demonstrated[9]. Such mixed excitations exist at low temperature in multiferroic manganites[9] and are suspected at room temperature in $BiFeO_3$[10]. Although in the former systems, electromagnons have been shown to depend on magnetic fields[11], their predicted sensitivity to electric fields, at the heart of their potential applicative interest, remains to be demonstrated.

In this paper, we focus on $BiFeO_3$(BFO), a special case among multiferroic materials. Indeed, BFO has a very high ferroelectric polarization reaching 100 μC/cm^2[12] below T_C = 1143 K and becomes an antiferromagnet below T_N = 643 K. The spins form a cycloid structure with a wavelength of λ_0 = 62 nm and an associated cycloid wavevector equal to $Q = 2\pi/\lambda_0$[13–15]. The magnetic cycloid lies in the (-12-1) plane, formed by the ferroelectric polarization ∥ [111] and the cycloid wavevector Q ∥ [10 − 1] (Fig. 1a). An electric field can simultaneously induce the flop of the polarization and the cycloidal plane[16]. The electrical switch of antiferromagnetic-ferroelectric domains in BFO has been observed[17,18] and controlled in a ferromagnet-multiferroic heterostructure[7]. Here we report direct electric-field control of spin wave states in BFO at room temperature.

In BFO, inelastic light scattering reveals two species of spin wave excitation modes. These are observed in Raman spectra as two series of sharp peaks labelled cyclon (ϕ_n) and extra cyclon modes (ψ_n) below 70 cm^{-1}, the frequency of the lowest phonon mode[10,19,20]. The cyclon ϕ_n and extra cyclon ψ_n modes correspond respectively to the spin oscillations in and out of the cycloidal plane (Fig. 1a) and their Raman scattering signature are reported in Fig. 1c. These two species of magnons originate from the translational symmetry breaking[21] of the cycloidal ground state. The spin wave momentum is no more conserved, and can be increased or decreased by a multiple of the cycloid wavevector Q. This leads to magnon zone folding at the Brillouin zone center, where ϕ_n and ψ_n correspond to magnon wavevector equal to $k = nQ$.

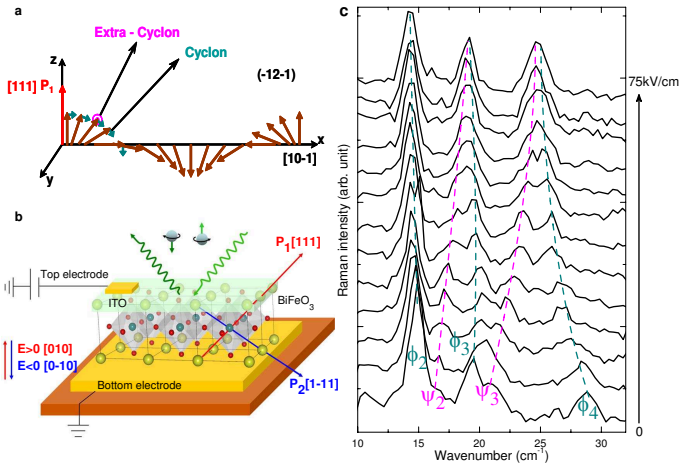

FIG. 1: **Electrical control of spin waves. a,** Depicts the spin cycloid ground state along with its low energy excitations when the ferroelectric polarization P_1 points along the [111] direction. The spin excitations correspond to in plane modes ϕ with an ellipsoidal shape elongated along y (cyclons) and out-of-plane modes ψ (extra-cyclons) as ellipse elongated along the tangent vector which belongs to the xz plane. **b,** Schematic diagram of the experimental set up used to apply an external electric field E to $BiFeO_3$ single crystals and to probe its spin excitations using Raman spectroscopy. The electrodes are deposited on the (010) plane. A positive (negative) electric field parallel to the [010] ([0-10]) direction allows the orientation of the ferroelectric moment P_1 (P_2) along the [111] ([1-11]) direction. Raman scattering is performed through the indium tin oxide (ITO) top electrode with light polarizations in the (010) plane. **c,** Raman spectra showing the magnon modes ϕ_2, ψ_2, ϕ_3, ψ_3 and ϕ_4 when the applied field ranges from 0 to 75 kV/cm. Dashed lines are guides to the eye following the shifts in frequency of each mode.

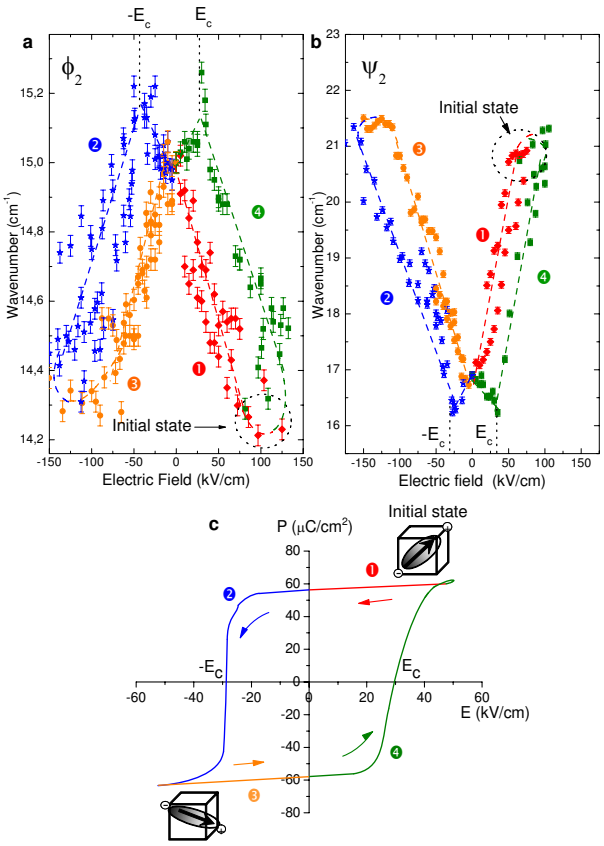

FIG. 2: **Spin wave hysteresis loop.** Voltage dependence of **a,** ϕ_2 and **b,** ψ_2 magnon modes. **c,** (P-E) hysteresis loop at room temperature. The shift of the spin wave frequencies follows the polarization loop along 1 (red diamond), 2 (blue star), 3 (orange circle) and 4 (green square).

The experimental set-up used to apply an electric field and to detect the optical excitations of spin waves is presented in Fig. 1b. The device consists of bottom and top (transparent) electrodes that enable the application of an electric field along the [010] and [0 − 10] directions of a bulk BFO sample. The effect of the external electric field on the spin wave modes is tracked in Fig. 1c. An external electric field applied along the [010] direction induces a blue shift of the ψ_n modes (ψ_2 and ψ_3) and a red shift of the ϕ_n modes (ϕ_2, ϕ_3, and ϕ_4). The promise of this electric-field control depends on our ability to selectively tune the spin wave states using the polarization hysteresis cycle and the switching of the polarization vector P.

Figures 2a,b show the frequency shift of the ϕ_2 (cyclon) and ψ_2 (extra-cyclon) modes as a function of the polarization cycle. This figure demonstrates that the spin wave modes are directly connected to the polarization hysteresis loop shown in Fig. 2c. With an initial polarization state $P_1 \parallel [111]$, decreasing the applied electric field ($E \parallel [010]$) induces an increase of the ϕ_2 mode frequency (red diamond, Fig. 2a) following path 1 in the polarization cycle. Traveling along path 2 with a negative electric field ($E \parallel$ [0-10]), the frequency of the ϕ_2 mode (blue star) increases up to the flip of P along the [1-11] direction (P_2) at critical electric field $E_c \approx -35$ kV/cm[12]. Beyond E_c, ϕ_2's frequency decreases. The hysteresis cycle can be completed along paths 3 and 4 leading to frequency shifts that are symmetric to the ones along 1 and 2. The ψ_2 mode is also directly connected to the polarization loop, but exhibits an opposite behaviour with respect to the ϕ_2 mode (Fig. 2b). The extra-cyclon mode ψ_2 presents a much stronger frequency shift under the effect of an electric field of 50 kV/cm, $\Delta\omega_{\psi_2} = (+2.1 \pm 0.1)$ cm^{-1}. Remarkably, the ψ_2 frequency is seen to increase by over 5 cm^{-1} at maximum E field, corresponding to a 30% shift of its natural frequency. This experiment clearly demonstrates the coupling between the spin waves and the ferroelectric character of the material and that a spin wave frequency hysteresis loop can be created and controlled at room temperature using the ferroelectric hysteresis loop.

There exists other methods for electric-field control of spin waves. Rado *et al.* detected a shift of the order of 3×10^{-5} cm^{-1} (relative shift of 0.01%) in lithium ferrite under the application of similar voltages[22]. Recently, Vlaminck and Bailleul demonstrated a doppler shift of

the order of 10^{-3} cm^{-1} (0.3%) using electric currents[23]. The present experiment shows that the coupling between magnetic and ferroelectric degrees of freedom provides a much more efficient method for electric-field control of spin waves, with frequency shifts over 5 cm^{-1} (30%), several orders of magnitude larger than with previous methods.

The strong spin wave frequency shifts that we observe may be interpreted as resulting from a combination of magnetoelectric interactions. The component of E along P (denoted E_z) cannot play any role because of the competition with the internal electric field parallel to $\hat{z}$ produced by P. Hence we only consider interactions involving $E_\perp = (E_x, E_y)$. The Dzyaloshinskii-Moriya (DM) interaction that couples E to $M \times L$ is allowed by the R3c crystal symmetry of BFO[24], and also induces a transition from the cycloidal to a homogeneous spin state at large $E_\perp$[25]. The DM interaction produces spin wave shifts that are independent of E at low electric field, at odds with the data, and that scale as $E_\perp^2$ at larger field[26]. Another class of magnetoelectric interactions, the so called flexoelectric interactions[25,27] couple E to gradients of L. For example, the flexoelectric interaction in a homogeneous magnet leads to an instability towards a spiral state and to spin wave shifts linear in $E_\perp$[27]. However, in our case of bulk BFO the magnetic order is a cycloid that is itself induced by terms that couple P to gradients of L and have the same form as the flexoelectric interaction[25,28]. Therefore, there is a competition between these different couplings that leads to a renormalization of the cycloid wavevector. Since both ω_ϕ and ω_ψ are directly proportional to the cycloid wavevector, a large $E_\perp$ will increase all spin wave frequencies by the same amount. Thus, the DM and the flexoelectric interactions are not able to reproduce the experimental data at lower field but might play a role at larger field.

Here, we have found that the spin wave frequency shifts can be interpreted using the Landau free energy model based on an additional kind of magnetoelectric interactions induced by the external electric field. Indeed, the R3c symmetry of BFO allows the presence of two linear magnetoelectric interactions that couple the Néel order parameter L directly with $E_\perp$,

Here, we have found that the spin wave frequency shifts can be interpreted using the Landau free energy model based on an additional kind of magnetoelectric interactions induced by the external electric field. Indeed, the R3c symmetry of BFO allows the presence of two linear magnetoelectric interactions that couple the Néel order parameter L directly with $E_\perp$,

$$F_1 = \frac{1}{2}\kappa_1 E_\perp \cdot L_\perp L_z, \quad (1)$$

$$F_2 = \frac{1}{2}\kappa_2 E_\perp \cdot \left[\left(L_y^2 - L_x^2\right)\hat{x} + 2L_x L_y \hat{y}\right], \quad (2)$$

with κ_1 and κ_2 phenomenological coupling constants. Physically, F_1 and F_2 model additional magnetic anisotropy energies induced by $E_\perp$. Hence their microscopic origin is related to spin-orbit coupling. The first interaction (F_1) produces a red shift for both ψ_n and ϕ_n modes when $E_\perp$ is increased. Thus, F_1 cannot explain the experimental observations at low $E_\perp$ (Fig. 2a,b). On the other hand, the interaction F_2 induces a blue shift for all ψ_n modes, and a red shift for ϕ_n modes with $n \geq 2$ as found experimentally, see Fig. 3. This interaction drives the system into a homogeneous state when $E_\perp$ becomes greater than a homogeneous critical field $E_{hs} \propto 1/\kappa_2$. The calculated curves show that cyclon and extra cyclon mode frequencies converge to two fixed points at the crit-

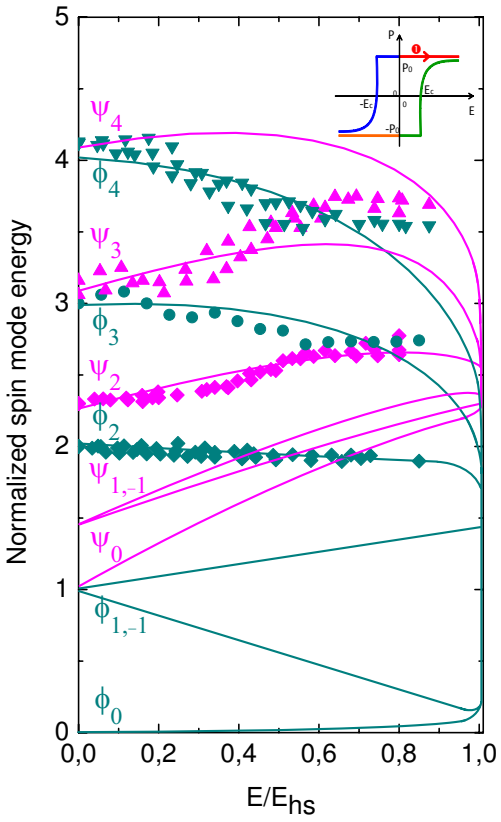

FIG. 3: **Electric field dependence of the measured and calculated spin wave frequencies.** When the applied electric field is zero, the energy of the ϕ_n and ψ_n modes are $E_{\phi_n} = nv_0Q$ and $E_{\psi_n} = \sqrt{1+n^2}v_0Q$ respectively, with index n labelling the modes, $v_0 = 1.4 \times 10^6$ cm/s the fundamental cyclon spin wave velocity, and Q the cycloid wavevector[10]. The figure shows the spin wave mode energies normalized to v_0Q as a function of the ratio of the applied electric field E divided by the electric field E_{hs} required to destroy the cycloid. When $E > E_{hs}$ the spin ground state becomes homogeneous in space. The closed symbols are the experimental data obtained following path 1 (insert) in the polarization cycle using $E \parallel [010]$ from 0 to 125 kV/cm : ϕ_2 (circle), ϕ_3 (diamond), ϕ_4 (down triangle), ψ_2 (star), ψ_3 (up triangle). (P is parallel to the [111] direction and no polarization flop occurs. Solid lines are explicit numerical calculations obtained from a dynamical Ginzburg-Landau theory based on the linear magnetoelectric interaction F_2.

ical field E_{hs}. A comparison between theory and experiment (Fig. 3) gives an estimate of $E_{hs} \approx 160$ kV/cm (above the maximum electric field of 125 kV/cm that could be applied to our sample without damage). Calculations are in good agreement with the experimental data in the low field region (see Fig. 3), but a clear deviation occurs at high fields. Interestingly, cyclon and extra cyclon modes seem to merge for $E > 0.5E_{hs}$. This effect and the difference between theory and experiment at high fields might be due to other magnetoelectric interactions such as the DM and the flexoelectric interactions discussed above.

The demonstration of electrical control of spin wave states represents a significant step towards making new spin wave-based technologies. The cyclon spin wave dispersion can be written as $\omega_\phi = v_\phi k$, and the extra-cyclon dispersion as $\omega_\psi = v_\psi\sqrt{k^2+Q^2}$. For $E = 0$, the spin wave velocities are equal, $v_\phi = v_\psi = v_0 = 1.4 \times 10^6$ cm/s[10]. However, under an electric field of 100 kV/cm the ϕ and ψ spin wave velocities are tuned by $\Delta v_\phi = -6 \times 10^4$ cm/s, and $\Delta v_\psi = +4 \times 10^5$ cm/s respectively. While the speed of electron spin precession in a magnetic field is generally fixed by intrinsic properties of the materials considered, our work shows that in a multiferroic the spin wave speed can be continuously adjusted and in a different way depending on the spin propagating mode by the applied electric fields.

We have demonstrated that the frequency of spin waves can been tuned electrically by over 30% at room temperature in multiferroic $BiFeO_3$. This electric-field dependence mimics that of the ferroelectric polarization, providing a handle for the non-volatile, low-power control of spin waves. Thus, aside from its potential for spintronics[29] and photonics[30], $BiFeO_3$ emerges as an exciting platform for testing novel magnonic device concepts, which further confirms it as a key multifunctional material for beyond-CMOS technology.

Methode

Experimental method

$BiFeO_3$ single crystals were grown in air using Bi_2O_3-Fe_2O_3 flux in an alumina crucible as detailed in ref[12]. and present a single ferroelectric and antiferromagnetic domain state. Polarized optical microscope images of the samples show that the crystal consists of one single ferroelectric domain[12]. Neutron measurements on the same samples have shown the presence of one antiferromagnetic domain[16]. A conducting Indium tin oxide (ITO) layer was grown by pulsed laser deposition on the top of the (010) sample surface to apply a uniform electric field. ITO has no Raman signal in the frequency range of interest. All the measurements were performed in vacuum at room temperature on several samples.

Raman scattering was performed on the (010) sample surface in backscattering geometry using the 647.1 nm laser line. Raman scattering is collected by a triple spectrometer Jobin Yvon T64000 equipped with a CCD. The spot size is about 100 μm^2 and the penetration depth is less than 10^{-5} cm. Reproducible Raman measurements have been performed on several points on the sample surfaces.

The ϕ_n and ψ_n modes (n index labels the modes from their lowest to highest energy) were selectively observed using parallel and crossed polarizations in the (010) plane, respectively (see Supplementary Information). The polarizations are defined with respect to the projection of the cycloid wavevector $Q \parallel$ [10-1] in the (010) plane (the direction of the wavevector Q is not directly accessible in the (010) plane). In order to show simultaneously several ϕ_n and ψ_n modes, Fig. 1b presents measurements without specific polarization.

Theoretical method

We consider a total free energy given by $F = F_0 + F_1 + F_2$, with F_0 the usual model free energy of multiferroic BFO[21,25],

$$F_0 = \frac{A}{2}L^2 + \frac{r}{2}M^2 + \frac{G}{4}L^4 + \frac{c}{2}\sum_{i=x,y,z}(\nabla L_i)^2 - \alpha_P P\cdot[L(\nabla\cdot L) + L\times(\nabla\times L)], \qquad (3)$$

and F_1, F_2 given by Eqs. (1) and (2) respectively [we omit the purely ferroelectric contributions to Eq. (3) because they play no role in the discussion below]. Here A, r, G, c, and α_P are phenomenological constants. The ground state is determined by the condition $\frac{\delta F}{\delta L} = 0$; when $E_\perp = 0$ the ground state is a harmonic cycloid $L_0 = L_0[\sin(Qx)\hat{x} + \cos(Qx)\hat{z}]$ with wavevector $Q = \frac{\alpha P}{c}$ and amplitude $L_0^2 = (-A + cQ^2)/G$. The effect of $E_\perp$ is to reduce the ground state wavevector Q and to add additional anharmonic contributions to L_0 at odd multiples of Q. When $E_\perp$ is equal to a critical field $E_{hs} = \frac{(\pi\alpha_P P)^2}{4c}\frac{1}{\kappa_2}$, the cycloid wavevector Q becomes equal to zero, signaling a transition to a homogeneous state.

The spin wave excitation frequencies are determined from the Landau-Lifshitz equations of motion. After combining the equations of motion for the order parameters L and M we get

$$\frac{\partial^2 L}{\partial t^2} = -r(\gamma L_0)^2\left[\frac{\delta F}{\delta L} - \left(\hat{L}_0\cdot\frac{\delta F}{\delta L}\hat{L}_0\right)\right], \qquad (4)$$

where γ is the gyromagnetic ratio. We find wave-like solutions by plugging in $L = L_0 + (\delta L)e^{i\omega t}$ in Eq. (4), with $(\delta L) = \phi(x)\hat{D} + \psi(x)\hat{y}$. The unitary vector $\hat{D}$ is tangential to L_0, i.e. it is orthogonal to L_0 but lies within the cycloid plane. Plugging $\phi(x) = \sum_n \phi_n e^{inQx}$, and $\psi(x) = \sum_n \psi_n e^{inQx}$ into Eq. (4) leads to a matrix equation whose eigenvalues give the spin wave excitations at $k = 0$.

We want to underline that the free energy model for BFO Eq. (3) does not contain any magnetic anisotropy. Nevertheless, the present experiment shows that an external E field induces magnetic anisotropy linear in E, see Eq. (2). In other words, the electric field activates a latent anisotropy in the material, leading to a large effect in the case of Eq. (2).

[1] Kruglyak, V. V., Demokritov, S. O. & Grundler, D. Magnonics. *J. Phys. D: Appl. Phys.* **43**, 264001 (2010).

[2] Kajiwara, Y. *et al.* Transmission of electrical signals by spin-wave interconversion in a magnetic insulator, *Nature* **464**, 262 (2010).

[3] Khitun, A., Bao, M. & Wang, K. L. Magnonic logic circuits. *J. Phys. D: Appl. Phys.* **43**, 264005 (2010).

[4] Schneider, T., Serga, A. A., Leven, B., Hillebrands, B., Stamps, R. L. & Kostylev, M. P. Realization of spin-wave logic gates. *Appl. Phys. Lett.* **92**, 022505 (2008).

[5] Catalan, G. & Scott, J. F., Physics and applications of bismuth ferrite. *Adv. Mater.* **21**, 2463, (2009).

[6] Eerenstein, W., Mathur, N. D. & Scott, J. F. Multiferroic and magnetoelectric materials. *Nature* **442**, 759-765 (2006).

[7] Chu, Y-H. *et al.* Electric-field control of ferromagnetism using a magnetoelectric multiferroic. *Nature Mater.* **7**, 478 (2008).

[8] Chappert, C., Fert, A. & Nguyen Van Dau, F. The emergence of spin electronics in data storage. *Nature Mater.* **6**, 813 (2007).

[9] Pimenov, A., Mukhin, A.A., Ivanov, V.Y., Balbashov, A.M. & Loidl A. Possible evidence for electromagnons in multiferroic manganites, *Nature Phys.* **2**, 97 (2006).

[10] Cazayous, M. *et al.* Possible observation of cycloidal electromagnons in $BiFeO_3$. *Phys. Rev. Lett.* **101**, 037601 (2008).

[11] Pimenov, A., Shuvaev, A.M., Mukhin, A.A. & Loidl, A. Electromagnons in multiferroic manganites. *J. Phys.: Condens. Matter.* **20**, 434209 (2008).

[12] Lebeugle, D. *et al.* Room-temperature coexistence of large electric polarization and magnetic order in $BiFeO_3$ single crystals. *Phys. Rev. B* **76**, 024116 (2007).

[13] Smolenski, G. A., Yudin, V. M., Sher, E. S. N. & Stolypin, Y. E. Antiferromagnetic properties of some perovskites. *Sov. Phys. JETP* **16**, 622 (1963).

[14] Lee, S. *et al.* Single ferroelectric and chiral magnetic domain of single-crystalline $BiFeO_3$ in an electric field. *Phys. Rev. B* **78**, 100101(R) (2008).

[15] Sosnowska, I., Peterlin-Neumaier, T. & Steichele, E. Spiral magnetic ordering in bismuth ferrite. *J. Phys. C* **15**, 4835 (1982).

[16] Lebeugle, D. *et al.* Electric-field-induced spin flop in $BiFeO_3$ single crystal at room temperature. *Phys. Rev. Lett.* **100**, 227602 (2008).

[17] Zhao, T. *et al.* Electrical control of antiferromagnetic domains in multiferroic $BiFeO_3$ films at room temperature. *Nature Mater.* **5**, 823 (2006).

[18] Baek, S. H. *et al.* Ferroelastic switching for nanoscale non-volatile magnetoelectric devices. *Nature Mater.* **9**, 309 (2010).

[19] Singh, M. K., Katiyar, R. & Scott, J. F. New magnetic phase transitions in $BiFeO_3$. *J. Phys. Condens. Mat.* **20**, 252203 (2008).

[20] Rovillain, P. *et al.* Polar phonons and spin excitations coupling in multiferroic $BiFeO_3$ crystals. *Phys. Rev. B* **79**, 180411(R) (2009).

[21] de Sousa, R. & Moore, J. E. Optical coupling to spin waves in the cycloidal multiferroic $BiFeO_3$. *Phys. Rev. B* **77**, 012406 (2008).

[22] Rado, G.T., Vittoria, C., Ferrari, J.M. & Remeika, J.P. Linear electric field shift of a ferromagnetic resonance: Lithium ferrite. *Phys. Rev. Lett.* **41**, 1253 (1978).

[23] Vlaminck, V. & Bailleul, M. Current-induced spin-wave doppler shift. *Science* **322**, 410 (2008).

[24] de Sousa, R. & Moore, J. E. Comment on "Ferroelectrically induced weak ferromagnetism by design". *Phys. Rev. Lett.* **102**, 249701 (2009).

[25] Sparavigna, A., Strigazzi, A. & Zvezdin, A. Electric-field effect on the spin-density wave in magnetic ferrolectrics. *Phys. Rev. B.* **50**, 2953 (1994).

[26] de Sousa, R. & Moore, J.E. Electrical control of magnon propagation in multiferroic $BiFeO_3$ films. *Appl. Phys. Lett.* **92**, 022514 (2008).

[27] Mills, D. L. & Dzyloshinskii, I. E. Influence of electric fields on spin waves in simple ferromagnets: role of the flexoelectric interaction. *Phys. Rev. B.* **78**, 184422 (2008).

[28] Zvezdin, A.K. & Pyatakov, A.P. Flexomagnetoelectric effect in bismuth ferrite. *Phys. Stat. Solidi B* **246**, 1956 (2009).

[29] Béa, H., Gajek, M., Bibes, M. & Barthélémy, A. Spintronics with multiferroics. *J. Phys.: Condens. Matter* **20**, 434221 (2008).

[30] Choi, T., Lee., S., Choi, Y.J., Kiryukhin, V. & Cheong, S.-W. Switchable ferroelectric diode and photvoltaic effect in $BiFeO_3$. *Science*, **324**, 63-66 (2009)

Acknowledgements

The authors would like to thank R. Lobo and P. Monod for fruitful discussions and E. Jacquet for technical assistance. DC, MB and AB would like to acknowledge support from the French Agence Nationale pour la Recherche, contract MELOIC (ANR-08-P196-36). RdS would like to acknowledge support from the Natural Sciences and Engineering Research Council of Canada.

Correspondence

Correspondence and requests for materials should be addressed to M. Cazayous (email: maximilien.cazayous@univ-paris-diderot.fr).